**Electronic Supplementary Material (ESI) for ChemComm.**

**This journal is © The Royal Society of Chemistry 2018**

# Supporting Information

## Nanoclay-induced defective g-C3N4 photocatalyst for highly efficient catalytic reaction

**Qihang Zhao[ab], Liangjie Fu[ab], Denghui Jiang[ab], Yunfei Xi[c] and Huaming Yang[abd]***

[a] *Department of Inorganic Materials, School of Minerals Processing and Bioengineering, Central South University, Changsha 410083, China.*

[b] *Hunan Key Lab of Mineral Materials and Application, Central South University, Changsha 410083, China*

[c] *School of Earth, Environmental and Biological Sciences, Queensland University of Technology, Brisbane, QLD 4001, Australia*

[d] *State Key Lab of Powder Metallurgy, Central South University, Changsha 410083, China*

*Corresponding author, Email: hmyang@csu.edu.cn, Fax: +86-731-888710804, Tel.:+86-731-88830549*

## Experimental section

**Materials.** Kaolinite was obtained from Kaolinite Clay Co., Ltd (Suzhou, China), and its chemical compositions were as follows: $SiO_2$ 53.27%, $Al_2O_3$ 42.46%, $SO_3$ 2.19%, $K_2O$ 0.54%, $Fe_2O_3$ 0.48%, $TiO_2$ 0.33%, $P_2O_5$ 0.26%, MgO 0.16%, CaO 0.09%, CuO 0.01%. Dimethyl sulfoxide (DMSO), urea, Orange II, NaCl, sodium azide ($NaN_3$), peroxymonosulfate (PMS, $KHSO_5 \cdot 0.5KHSO_4 \cdot 0.5K_2SO_4$)**,** ammonium oxalate (AO) that-Butanol (TBA) and methanol (MeOH) were purchased from Sinopharm Chemical Reagent Co. Ltd. (China) and without further purification.

**Preparation of g-$C_3N_4$.** The pristine g-$C_3N_4$ sample was prepared by using thermal polymerization of urea in high temperature. Typically, 10 g of urea was put in a crucible with a cover, and heated at 550 °C for 3 h with the ramping rate of 5 °C/min. After the samples cooled down, the resultant milk white agglomerates were obtained by washing with ethanol and deionized water for several times.

**Preparation of $C_3N_4$/Kaol.** Dimethyl sulfoxide (DMSO) intercalation into kaolinite (Kaol) was performed by adding 10 g of kaolinite to the mixture (90 mL of DMSO and 10 mL of water), and the above suspension was stirred at 60 °C for 4 h. For the DMSO-Kaol sample, it was obtained by washing with ethanol and deionized water for several times and dried at 60 °C. The U-DMSO-Kaol was prepared by mixing 1 g of pre-intercalation samples of DMSO-Kaol with different amounts of urea (5, 10, 15 g) and 0.1 mL $H_2O$ and fully ground, then it was placed in the oven and kept there for 12 h at 95 °C. The U-DMSO-Kaol was placed in a crucible with a cover and heated at 550 °C for 3 h with the ramping rate of 5 °C/min. After the samples being cooled down, the powers were obtained by being washed with ethanol and deionized water for several times. Through the above steps, the product denoted 5$C_3N_4$/Kaol, 10$C_3N_4$/Kaol and 15$C_3N_4$/Kaol**.**

**Preparation of U-$C_3N_4$/Kaol.** The U-Kaol was prepared by mixing 1 g of kaolinite with urea 10 g and 0.1 mL $H_2O$ and fully ground, then it was placed in the oven and kept there for 12 h at 95 °C. The U-Kaol was placed in a crucible with a cover and heated at 550 °C for 3 h with the ramping rate of 5 °C/min. After the samples being cooled down, the powers were obtained by washing with ethanol and deionized water for several times, the product denoted U-$C_3N_4$/Kaol.

**Preparation of g-$C_3N_4$+Metakaol.** The kaolinite was placed in a crucible with a cover and heated at 550 °C for 3 h with the ramping rate of 5 °C/min. After the samples being cooled down, the metakaolinite were obtained by being washed with ethanol and deionized water for several times. The g-$C_3N_4$+Metakaol was prepared by mixing 1 g of metakaolinite with g-$C_3N_4$ and fully ground.

**Preparation of $C_3N_4$/Kaol (400-600°C).** The kaolinite was placed in a crucible and heated at certain temperature (400, 500, 600 °C) for 3 h, respectively, the product denoted Kaol (400 °C), Kaol (500 °C), Kaol (600 °C).

The $C_3N_4$/Kaol (400 °C) was prepared by mixing 1 g of Kaol (400 °C) with urea 10 g and 0.1 mL $H_2O$ and fully ground, then it was placed in the oven and kept there for 12 h at 95 °C. The Kaol was placed in a crucible with a cover and heated at 550 °C for 3 h with the ramping rate of 5 °C/min. After the samples being cooled down, the powers were obtained by washing with ethanol and deionized water for several times.

The $C_3N_4$/Kaol (500 °C) was prepared by mixing 1 g of Kaol (500 °C) with urea 10 g and 0.1 mL $H_2O$ and fully ground, then it was placed in the oven and kept there for 12 h at 95 °C. The Kaol was placed in a crucible with a cover and heated at 550 °C for 3 h with the ramping rate of 5 °C/min. After the samples being cooled down, the powers were obtained by washing with ethanol and deionized water for several times.

The $C_3N_4$/Kaol (600 °C) was prepared by mixing 1 g of Kaol (600 °C) with urea 10 g and 0.1 mL $H_2O$ and fully ground, then it was placed in the oven and kept there for 12 h at 95 °C. The Kaol was placed in a crucible with a cover and heated at 550 °C for 3 h with the ramping rate of 5 °C/min. After the samples being cooled down, the powers were obtained by washing with ethanol and deionized water for several times.

**Characterizations.** The phase structure was analyzed by XRD (Bruker D8) using Cu K$\alpha$ radiation. Geometric morphology and element distribution were obtained scanning electron microscopy (SEM, FEI Quanta650) and transmission electron microscopy (TEM, FEI Tecnai

G2 f2). Atomic force microscopy (AFM) was performed by Veeco D3100. The chemical compositions and surface states of the samples were analyzed by X-Ray photoelectron spectroscopy (XPS), which were carried out on a Thermo Escalab 250Xi photoelectron spectrometer. The $N_2$ adsorption-desorption isotherms were measured at 77 K operated at a Micrometrics ASAP 2020. Solid-state $^{13}C$, $^{27}Al$ and $^{29}$ Si NMR spectra were performed on a Bruker Avance III 400 MHz instrument at room temperature. The electron spin resonance (ESR) were carried out using a Bruker EMX plus model spectrometer at ambient temperature under visible light irradiation. The UV-vis absorption spectra were measured using a spectrophotometer (Shimadzu UV-2700) in the range of 200 ~ 800 nm. Fourier transform infrared spectroscopy (FTIR) was measured on a Bruker Tensor 27 spectrophotometer. The electron paramagnetic resonance (EPR) measurements were measured on a Bruker Model A300 spectrometer. Elemental analysis was performed by a Vario EL III elemental analyzer. The NETZSCH STA 449F3 analyzer was applied to obtain Thermogravimetric (TG) analysis. Steady-state photoluminescence (PL) spectra were measured on a PE LS55 with the excitation light at 400 nm. The transient photocurrent performance was performed using a lock-in amplifier amplifier (SR 830, Stanford Research Systems, Inc.) with a light chopper (SR540, Stanford Research Systems, Inc.).

**Catalytic activity test.** For the organic pollutant degradation process, Orange II dye was selected as model pollutant. In a typical test, 15 mg of catalyst was first added to 30 mL of Orange II solution with an initial concentration of 50 mg/L at room temperature without pH adjustment. Then the suspension as stirred for 15 min to establish the adsorption–desorption equilibrium, followed by adding amounts of PMS solution to trigger the reaction. At various time intervals, 1 mL of mixture solution was extracted from the reactor. The concentration of Orange II ($\lambda$=486 nm) was determined by using UV-vis spectrometer.

**Photocatalytic activity test.** For the organic pollutant degradation process, Orange II dye was selected as model pollutant. In a typical test, 15 mg of catalyst was first added to 30 mL of Orange II solution with an initial concentration of 50 mg/L at room temperature without pH adjustment. Then the suspension was stirred for 15 min to establish the adsorption–desorption equilibrium, followed by adding amounts of PMS solution and simultaneously opening visible light (≥ 420 nm) to trigger the reaction. At various time intervals, 1 mL of mixture solution was extracted from the reactor. The concentration of Orange II ($\lambda$=486 nm) was determined by using UV-vis spectrometer.

## SEM, TEM and AFM images

As shown in Fig. S3 (a, b and c), it was clear that the colors of the powers have the obvious distinction, which leads to differences in the physicochemical properties. The SEM and TEM images (Fig. S3d.g and S3e.h) reveal that the metakaolinite and g-$C_3N_4$ possess a lamellar structure with a hexagonal appearance and sheet-like structure with the abundant porous structure, respectively. It is noticeable that 10$C_3N_4$/Kaol shows an analogous layered structure with metakaolinite and a rough surface (Fig. S3f). The results in Fig. S3i clearly signify that g-$C_3N_4$ with a loose and soft morphology are attached to the surface of metakaolinite. In addition, the energy dispersive X-ray spectroscopy (EDS) elemental mapping (Fig. S4) displays well-distributed soft g-$C_3N_4$ and further confirms the existence of C, N, Si, Al and O element and the contacts to each other. What's more, from results of the EDX elemental analysis, it is found that the contents of C and N are more than the ones of Si and Al, which demonstrate the homogeneous distribution of g-$C_3N_4$ on the surface of clay mineral. Atomic force microscopy (AFM) images and the corresponding height profiles are illustrated in Fig. S5. 10$C_3N_4$/Kaol photocatalyst exhibits a thinner thickness compared to g-$C_3N_4$ sample, which could be attributed to the confinement effect on the interlamination of kaolinite.[1] The subtle differences partly reflect the thickness of different samples. The randomly measured g-$C_3N_4$ and 10$C_3N_4$/Kaol possess similar thickness.

## XPS Data

To further investigated the chemical environment between metakaolinite and g-$C_3N_4$ and the surface/interfacial interactions in 10$C_3N_4$/Kaol, XPS spectra were performed and clearly showed C, N, Al, Si, and O element in the different samples (Fig. S7a). Furthermore, both g-$C_3N_4$ and 10$C_3N_4$/Kaol show typical binding energy states of carbon in graphitic carbon nitride (Fig. S7e). For the C 1s spectrum of g-$C_3N_4$, the binding energy shows three carbon species:

288.3 eV ($sp^2$-bonded carbon N-C=N), 285.5 eV ($sp^3$-coordinated carbon bonds C-N) and 284.8 eV (carbon-containing contaminants C-C or C=C).[2] Meanwhile, as displayed in Fig. S6f, N 1s XPS spectra of g-$C_3N_4$ show three peaks centered at 398.7, 399.5 and 401 eV, assigned to the C-N=C, N-C (3) and N-H, respectively. Moreover, the peak at 404.4 eV is attributed to the charging effects or positive charge localization in heterocycles.[3] More importantly, as shown in Fig. S7d, the shifting towards higher binding energy of Al 2p was observed in 10$C_3N_4$/Kaol compared to metakaolinite, which was resulted from the decrease of the electron concentration, confirming slight changes of Al atoms and the emergence of chemical bonds between g-$C_3N_4$ and metakaolinite.[4] However, it should be noted that the Si 2p peak of metakaolinite and 10$C_3N_4$/Kaol showed no obvious shift (Fig. S7d). In addition, as illustrated in Fig. S7b, no signal belonging to S 2p was detected from both metakaolinite and 10$C_3N_4$/Kaol. This result excludes the possibility of S-doping g-$C_3N_4$ in binary nanohybrid and further confirms that the DMSO acts as intercalator only for the intercalation reaction rather than reactant for the formation of cyano groups (Fig. S9). It is worthwhile that, compared to pure g-$C_3N_4$, the increasing ratio value of the N-C (3)/C and the C-N=C/C ratio decreased, which can be taken as strong evidence for the emergence of C-N=C vacancies resulted from the formation of cyano groups on the surface of 10$C_3N_4$/Kaol (Table S1).

## FTIR Spectra Data

As shown in Fig.S8b, the samples had the basic characteristic peaks of kaolinite. In detail, the characteristic peaks at 3697, 3665 and 3647 $cm^{-1}$ are related to the inner surface hydroxyls. In addition, the band at 3621 and 912 $cm^{-1}$ corresponds to the stretching of inner hydroxyl and Al-OH bending vibration, respectively. Since metakaolinite was generated by calcination of the kaolinite at 550 °C, the bands at 466 $cm^{-1}$ and 810 $cm^{-1}$ is related to a bending vibration of the Si–O group and tetrahedral coordinated of Al–O stretching vibration, respectively.[5] The absorption peak at 1068 $cm^{-1}$ is attributed to asymmetry stretching vibration of Si–O–X (X= tetra-coordinated Si or Al). For the mentioned peaks ahead, the absorption intensity obviously decreased with increasing the thermal treating temperature, suggesting that hydroxyl groups on the kaolinite surface are disappeared and the Si-O and Al-O groups are observed at high temperature.

## $N_2$ Adsorption/Desorption Isotherm Data

$N_2$ physisorption measurements were applied to evaluate the effect of g-$C_3N_4$ addition on the specific surface area and pore structure. Brunauer-Emmett-Teller (BET) surface area (Table S3) of the g-$C_3N_4$ is ca. 77.2 $m^2/g$ due to its thin, wrinkled and numerous pores property, which is almost four times higher than that of nanoclay kaolinite (ca. 19.6 $m^2/g$). And the specific surface area of the $C_3N_4$/Kaol samples increases progressively with adding urea mass from 5 g to 15 g, which are ascribed to the intimate integration between 2D g-$C_3N_4$ and 2D kaolinite to generate unique architecture (Fig. S10a). All the samples possess the similar isotherms, which imply the coexistence of micro- and mesoporosity. As shown in Fig. S10b, the pore size determined by the BJH method exhibit that they have mainly distributed in about 3 nm for all the samples.

## Catalytic Mechanism

To understand the activation/oxidation mechanism, the possible reactive radical species produced in activation of PMS were detected and presented in (Fig. S12c, S12d). In this case, a remarkable decrease in reaction rate is led by the existence of TBA and sodium azide ($NaN_3$) in the reaction system, fairly correlated with their higher addition quantity, which confirming the involvement of hydroxyl radical ($OH^{\bullet-}$) and singlet oxygen ($^1O_2$) in the catalytic reaction system. The generation of $^1O_2$ could be resulted from the defect site (-C≡N) interact with peroxymonosulfate through nucleophilic displacement of the O-O bond in $SO_4^{2-}$ or that defect-rich 10$C_3N_4$/Kaol with the delocalized π-electrons which could activate PMS during the reaction processes.[6]

# References

1. W. Liu, S. Xu, S. Guan, R. Liang, M. Wei, G. Evans David and X. Duan, *Adv. Mater.,* 2017, **30**, 1704376.

2. G. Zhang, Z. Wu, H. Liu, Q. Ji, J. Qu and J. Li, *Small*, 2017, **13**, 1702225.

3. K. Schwinghammer, M. B. Mesch, V. Duppel, C. Ziegler, J. Senker and B. V. Lotsch, *J. Am. Chem. Soc.*, 2014, **136**, 1730-1733.

4. M. Long, Y. Zhang, Z. Shu, A. Tang, J. Ouyang and H. Yang, *Chem. Commun.,* 2017, **53**, 6255-6258.

5. Y. Zhang, M. Long, P. Huang, H. Yang, S. Chang, Y. Hu, A. Tang and L. Mao, *Nano Res.*, 2017, **10**, 2633-2643.

6. W.-D. Oh, Z. Dong and T.-T. Lim, *Appl.Catal. B Environ.,* 2016, **194**, 169-201.

**Table S1** Summarized XPS data for g-$C_3N_4$ and 10$C_3N_4$/Kaol

| Sample | N-C=N | C-N | C-C<br>C=C | N-H | N-C (3) | C-N=C | N-H/C | N-C (3)/C | C-N=C/C |
|---|---|---|---|---|---|---|---|---|---|
| g-$C_3N_4$ | 288.3 | 285.5 | 284.8 | 401 | 399.5 | 398.7 | 0.09 | 0.15 | 0.67 |
| 10$C_3N_4$/Kaol | 288.4 | 285.7 | 284.7 | 401 | 399.8 | 398.8 | 0.08 | 0.17 | 0.58 |

**Table S2** The Si/Al ratio of metakaolinite and C/N ratios of g-$C_3N_4$ and 10$C_3N_4$/Kaol powders obtained by EA and XPS analysis

| Samples | EA | | | XPS | |
|---|---|---|---|---|---|
| | N (%) | C (%) | N/C | N/C | Si/Al |
| Metakaol | | | | | 1.12 |
| g-$C_3N_4$ | 59.61 | 36.66 | 1.39 | 0.86 | |
| 10$C_3N_4$/Kaol | 15.55 | 8.63 | 1.54 | 0.79 | 1.11 |

**Table S3** Surface area of the different sample

| Samples | Kaol | 5$C_3N_4$/Kaol | 10$C_3N_4$/Kaol | 15$C_3N_4$/Kaol | g-$C_3N_4$ |
|---|---|---|---|---|---|
| Surface area $m^2/g$ | 19.6 | 27.8 | 41.4 | 50.4 | 77.2 |

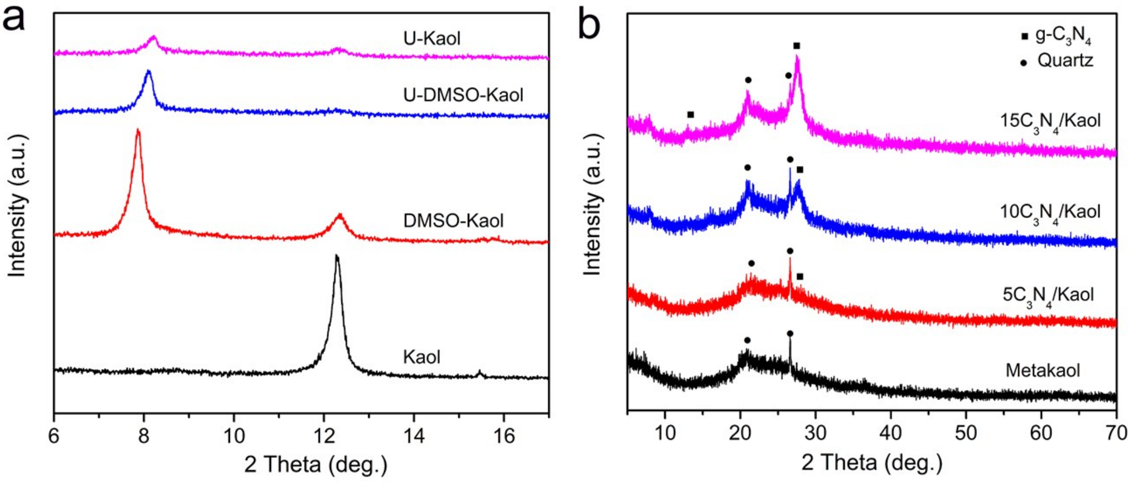

**Fig. S1** (a) XRD patterns of different samples; (b) XRD patterns of different samples.

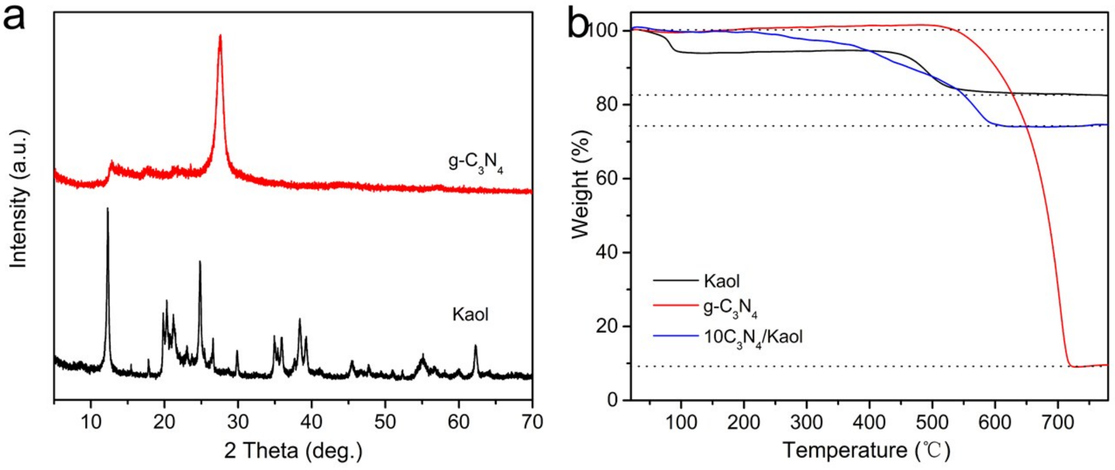

**Fig. S2** (a) XRD pattern of kaolinite and g-$C_3N_4$; (b) TG curves of different samples.

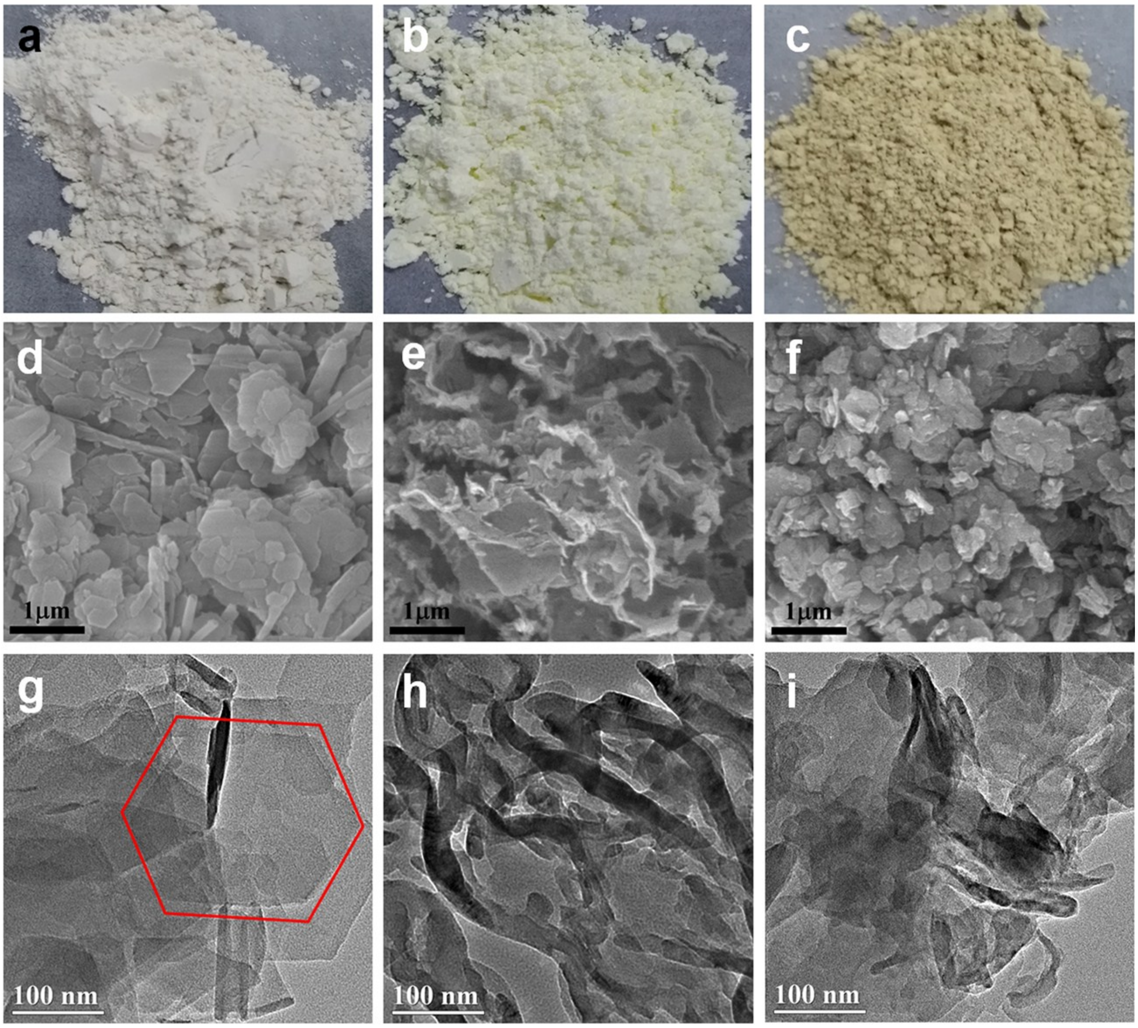

**Fig. S3** (a, b, c) Photographs; (d, e, f) SEM images; (g, h, i) TEM images of metakaolinite, g-$C_3N_4$ and $10C_3N_4$/Kaol, respectively.

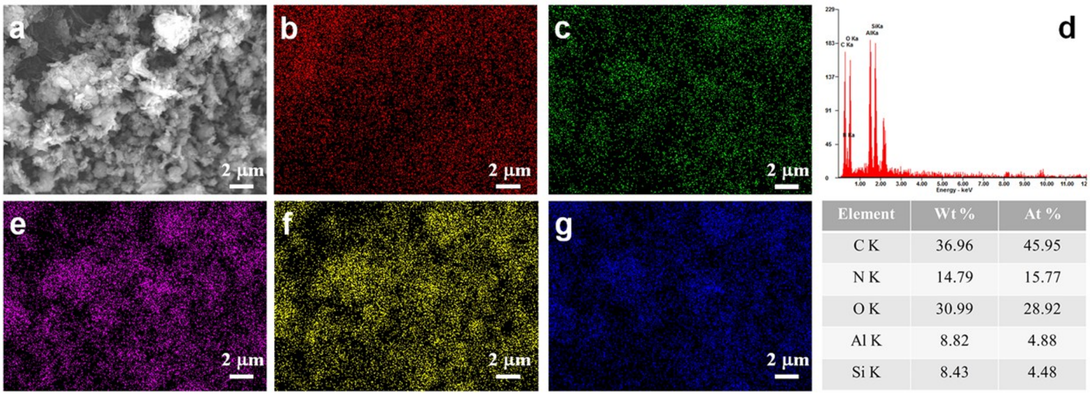

| Element | Wt % | At % |
|---|---|---|
| C K | 36.96 | 45.95 |
| N K | 14.79 | 15.77 |
| O K | 30.99 | 28.92 |
| Al K | 8.82 | 4.88 |
| Si K | 8.43 | 4.48 |

**Fig. S4** (a) SEM image of $10C_3N_4$/Kaol; EDS elemental mapping of (b) C; (c) N; (e) Si; (f) Al and (g) O for $10C_3N_4$/Kaol and EDX elemental analysis results of (a), respectively.

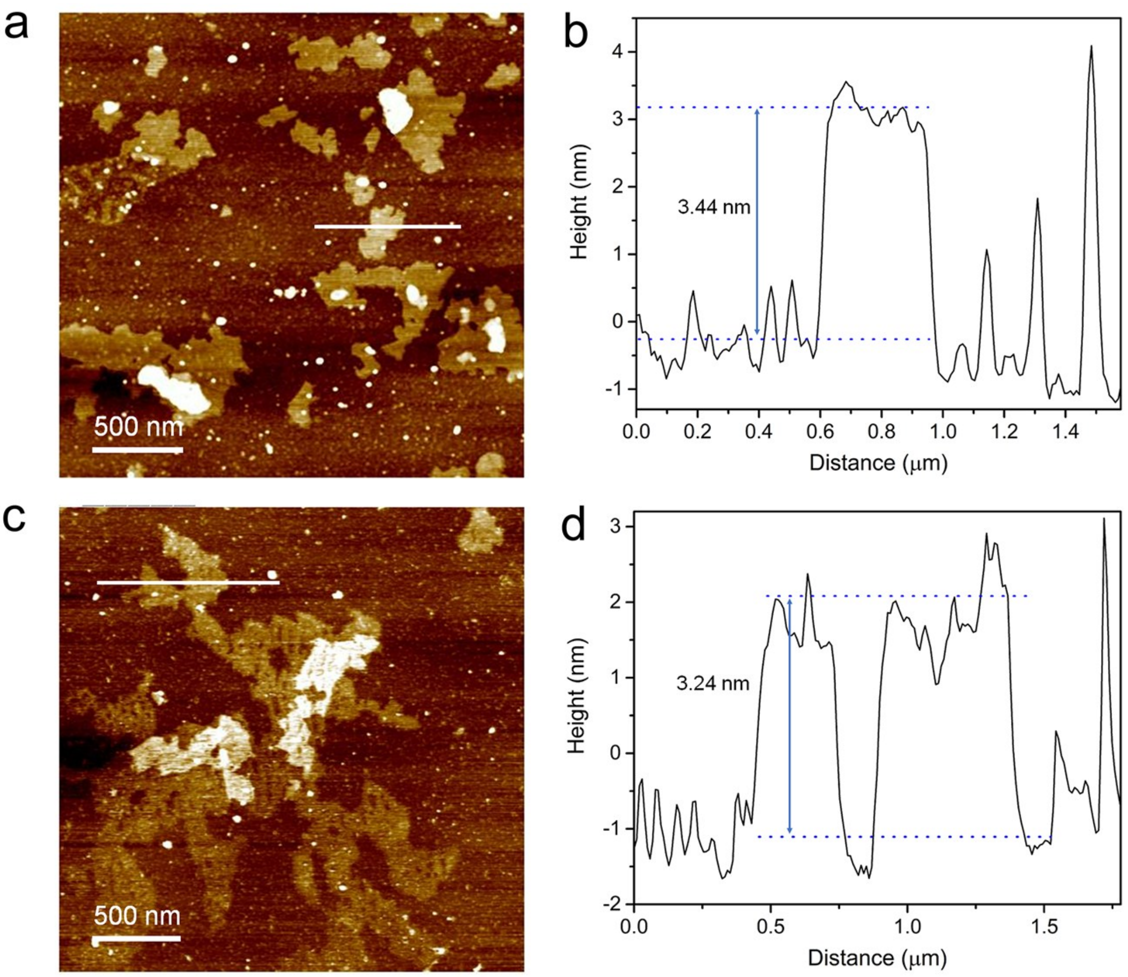

**Fig. S5** (a)AFM image and (b) corresponding height of g-$C_3N_4$, (c) AFM image and (d) corresponding height of 10$C_3N_4$/Kaol.

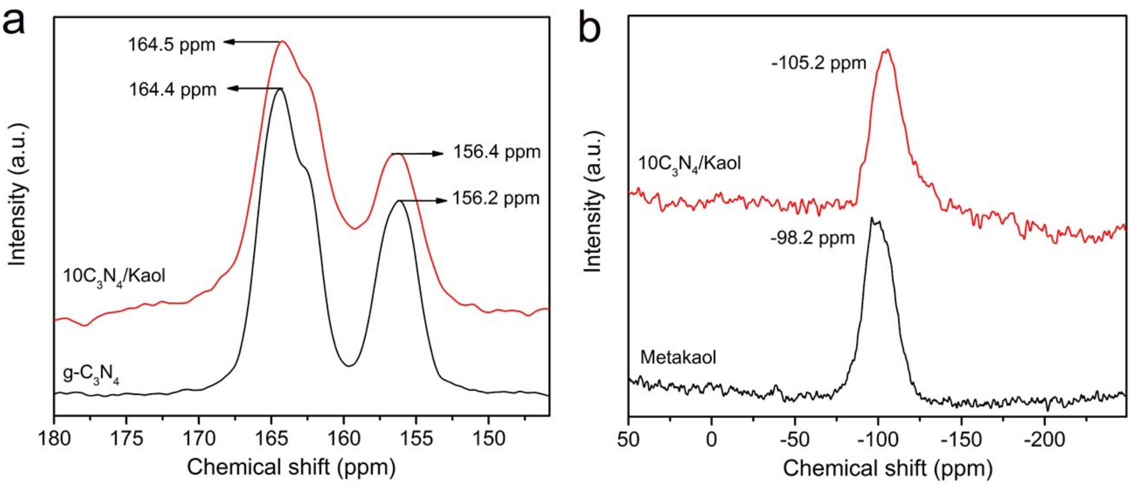

**Fig. S6** (a) The enlarged view of Solid-state $^{13}$C MAS NMR spectra of g-$C_3N_4$ and 10 $C_3N_4$/Kaol; (b) Solid-state $^{29}$Si MAS NMR spectra of metakaolinite and 10$C_3N_4$/Kaol.

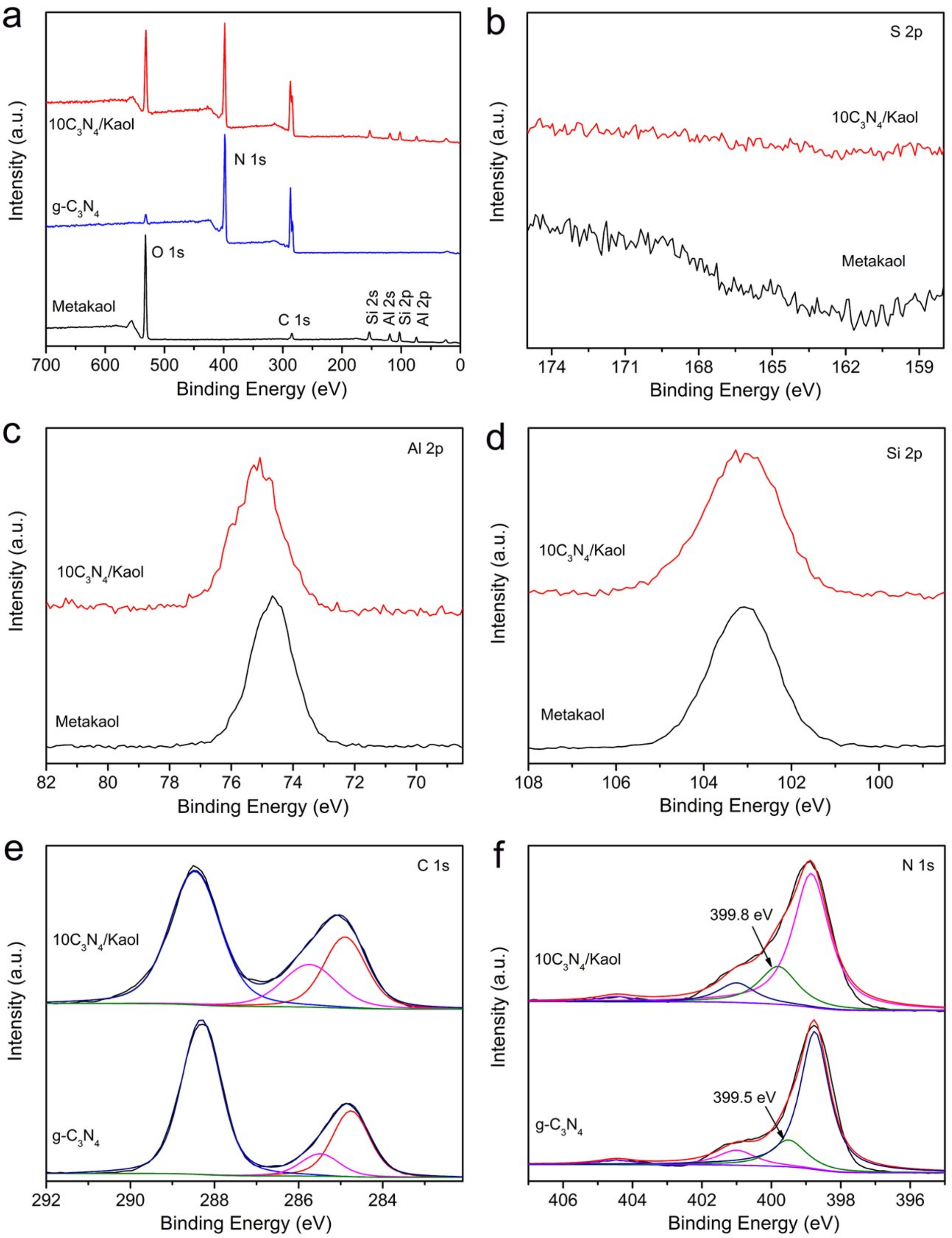

**Fig. S7** (a) XPS spectra of metakaolinite, g-$C_3N_4$ and 10$C_3N_4$/Kaol; (b) XPS spectra of S 2p of metakaolinite and 10$C_3N_4$/Kaol; (c) XPS spectra of Al 2p of metakaolinite and 10$C_3N_4$/Kaol; (d) XPS spectra of Si 2p of metakaolinite and 10$C_3N_4$/Kaol; (e) XPS spectra of C 1s of g-$C_3N_4$ and 10$C_3N_4$/Kaol; (f) XPS spectra of N 1s of g-$C_3N_4$ and 10$C_3N_4$/Kaol.

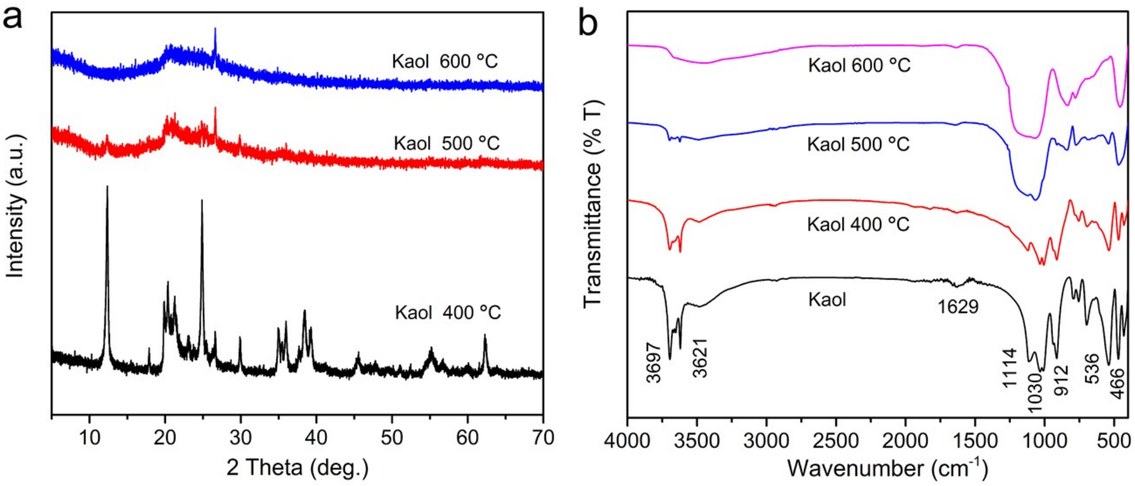

**Fig. S8** (a) XRD pattern of kaolinite (400 °C), kaolinite (500 °C) and kaolinite (600 °C); (b) FTIR spectra of kaolinite, kaolinite (400 °C), kaolinite (500 °C) and kaolinite (600 °C).

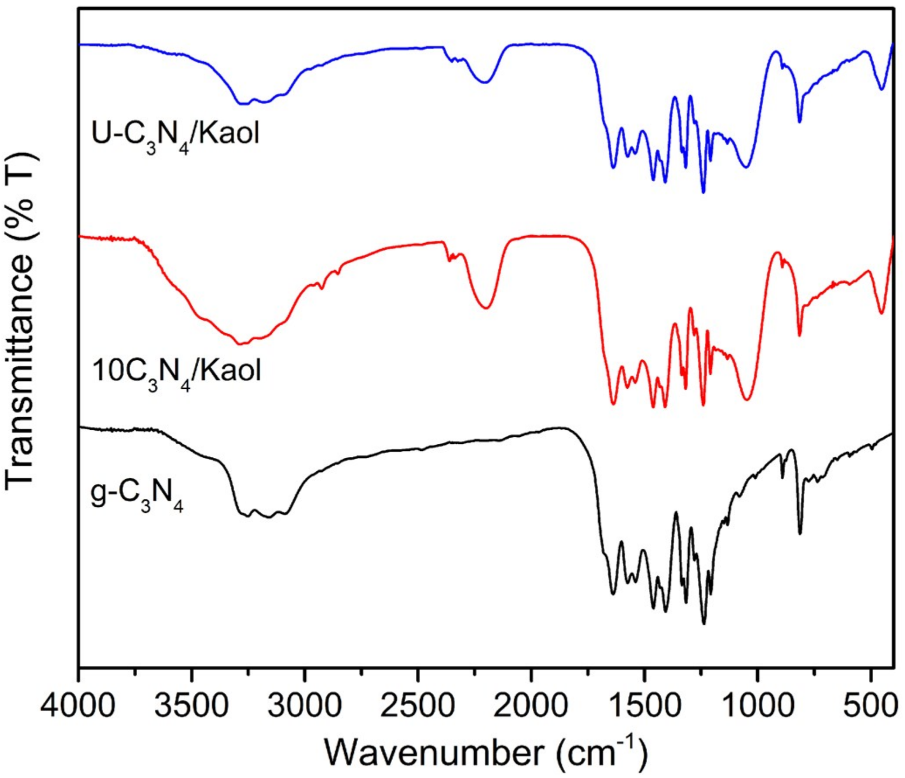

**Fig. S9** FTIR spectra of g-$C_3N_4$,10$C_3N_4$/Kaol and U-$C_3N_4$/Kaol

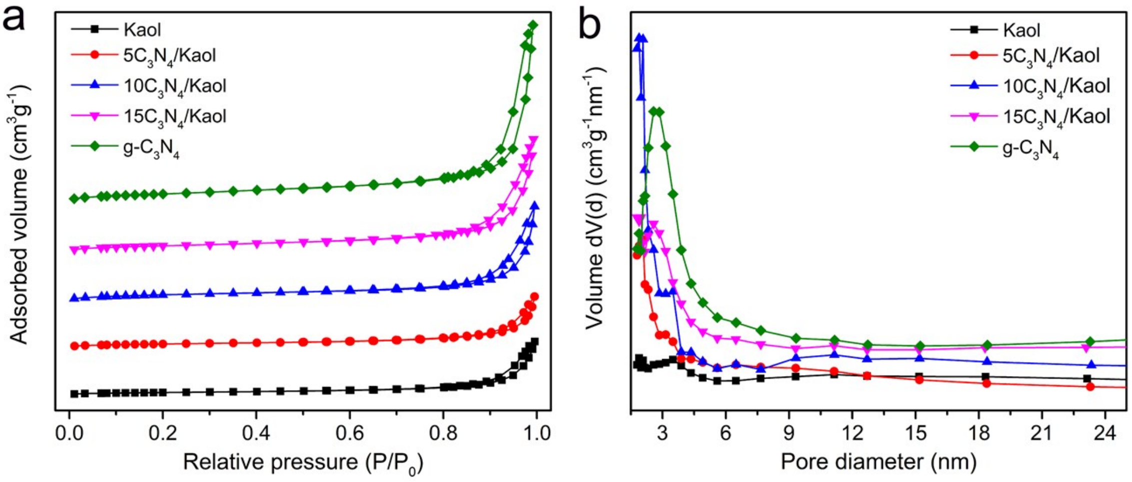

**Fig. S10** (a) $N_2$ adsorption-desorption isotherms of kaolinite, $5C_3N_4$/Kaol,$10C_3N_4$/Kaol, $15C_3N_4$/Kaol and g-$C_3N_4$; (b) Pore diameter distribution of kaolinite, $5C_3N_4$/Kaol,$10C_3N_4$/Kaol, $15C_3N_4$/Kaol and g-$C_3N_4$.

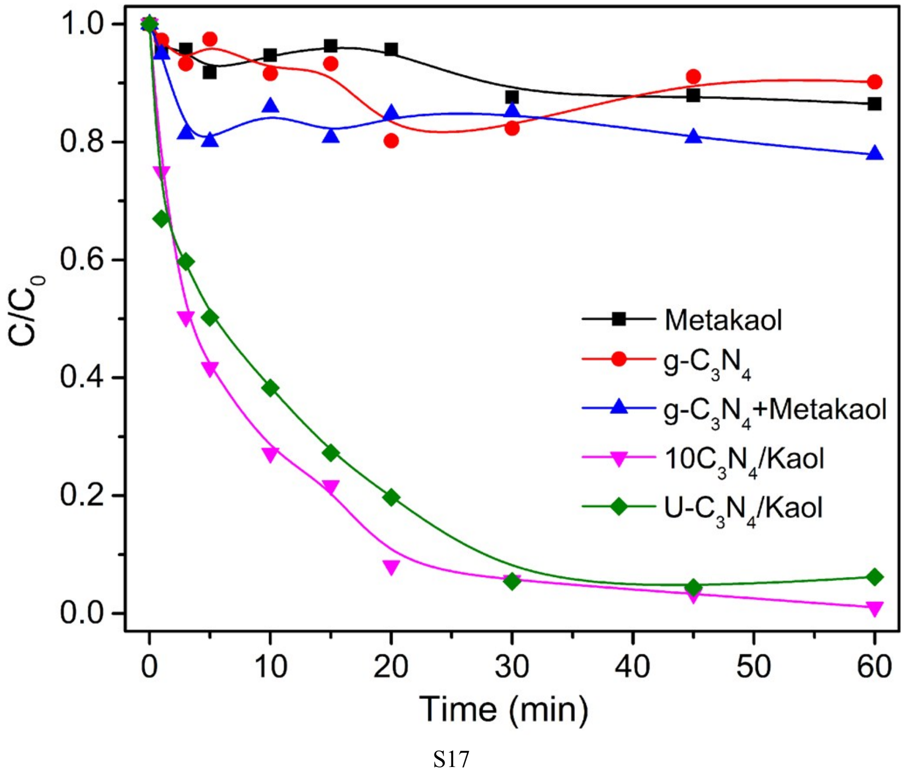

**Fig. S11** Removal efficiency of Orange II in different catalyst reaction systems. Reaction conditions: [Orange II] = 50 mg/L, [PMS] = 0.5 g/L, [Catalyst] = 0.5 g/L.

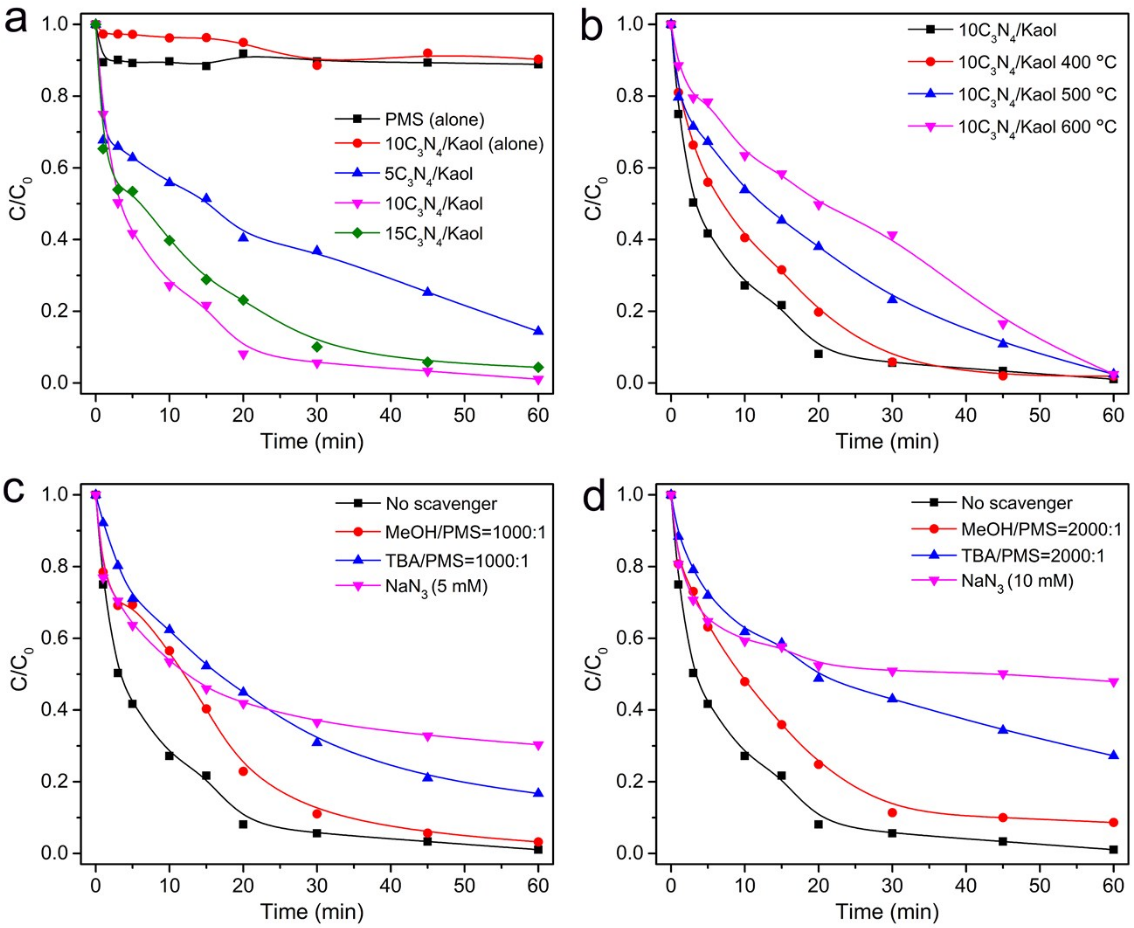

**Fig. S12** (a) and (b) Removal efficiency of Orange II in different catalyst reaction systems without visible light irradiation; (c) and (d) Effects of different scavengers on Orang II degradation in the presence of $10C_3N_4$/Kaol without visible light irradiation. Reaction conditions: [Orange II] = 50 mg/L, [PMS] = 0.5 g/L, [Catalyst] = 0.5 g/L.

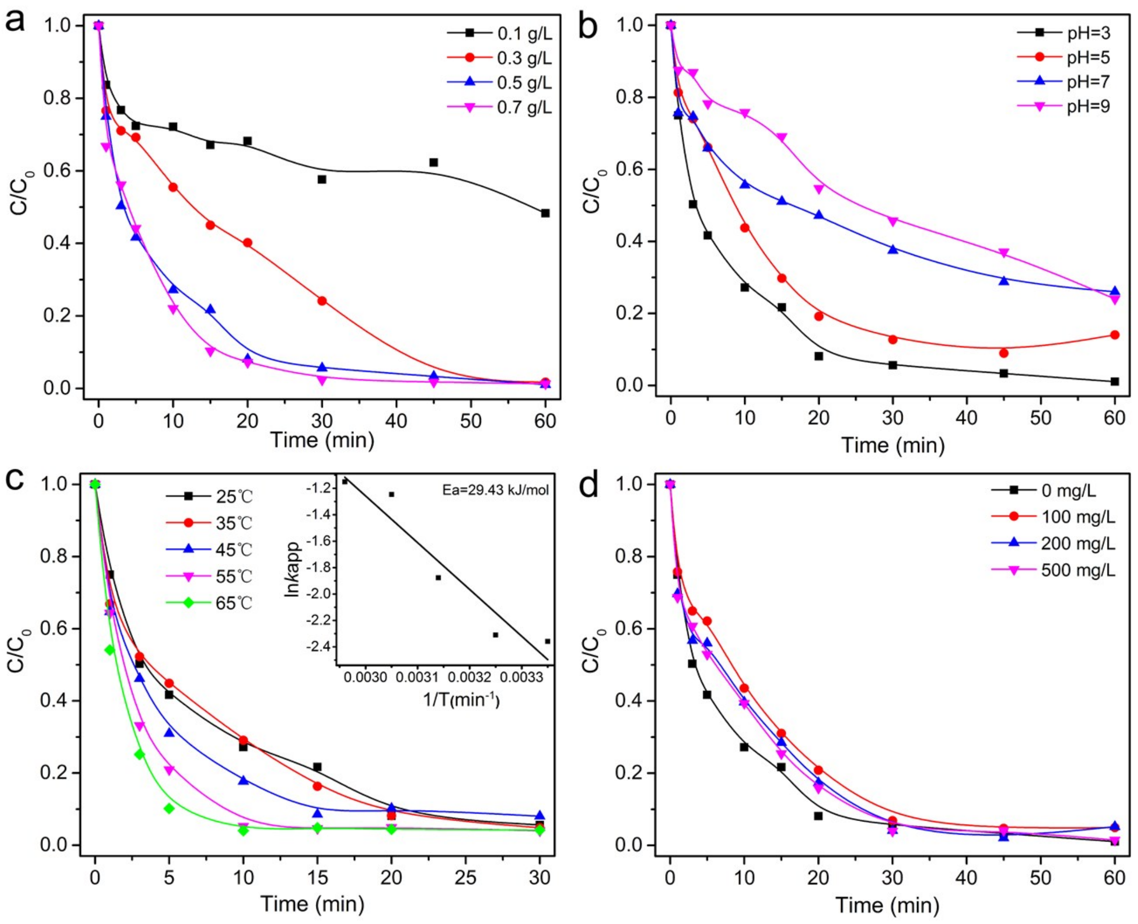

**Fig. S13** (a) Effect of catalyst dosages on Orange II removal; (b) Effect of solution pH on Orange II removal; (c) Effect of reaction temperatures on Orange II removal; (d) Effect of concentration of chloride ions on Orange II removal. Reaction conditions: [Orange II] = 50 mg/L, [PMS] = 0.5 g/L, [Catalyst ($10C_3N_4$/Kaol)] = 0.5 g/L.

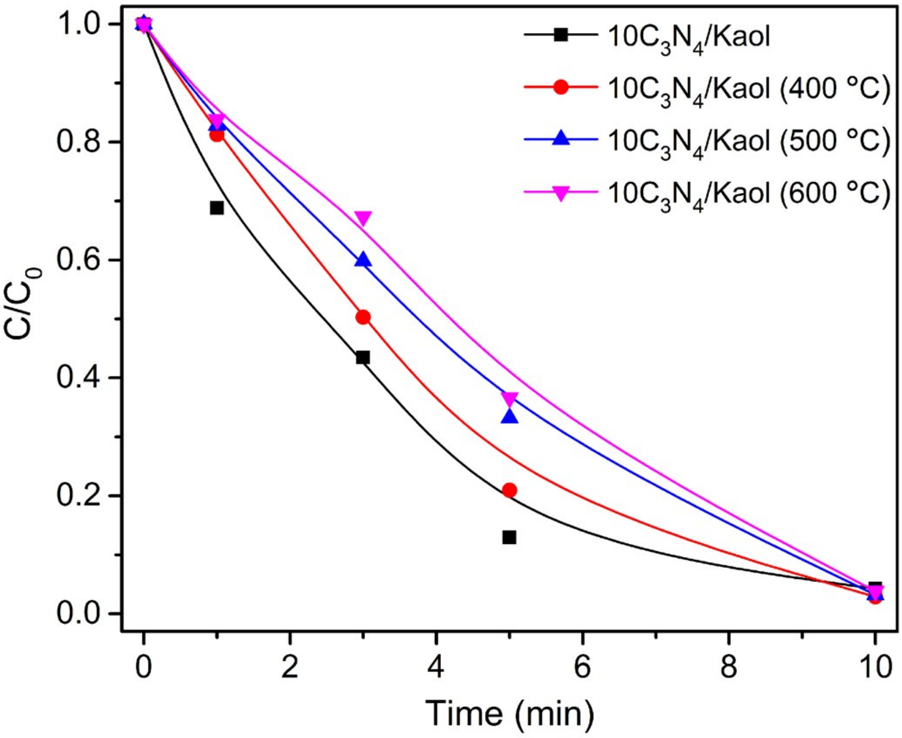

**Fig. S14** Removal efficiency of Orange II in different catalyst reaction systems under visible light irradiation. Reaction conditions: [Orange II] = 50 mg/L, [PMS] = 0.5 g/L, [Catalyst] = 0.5 g/L.

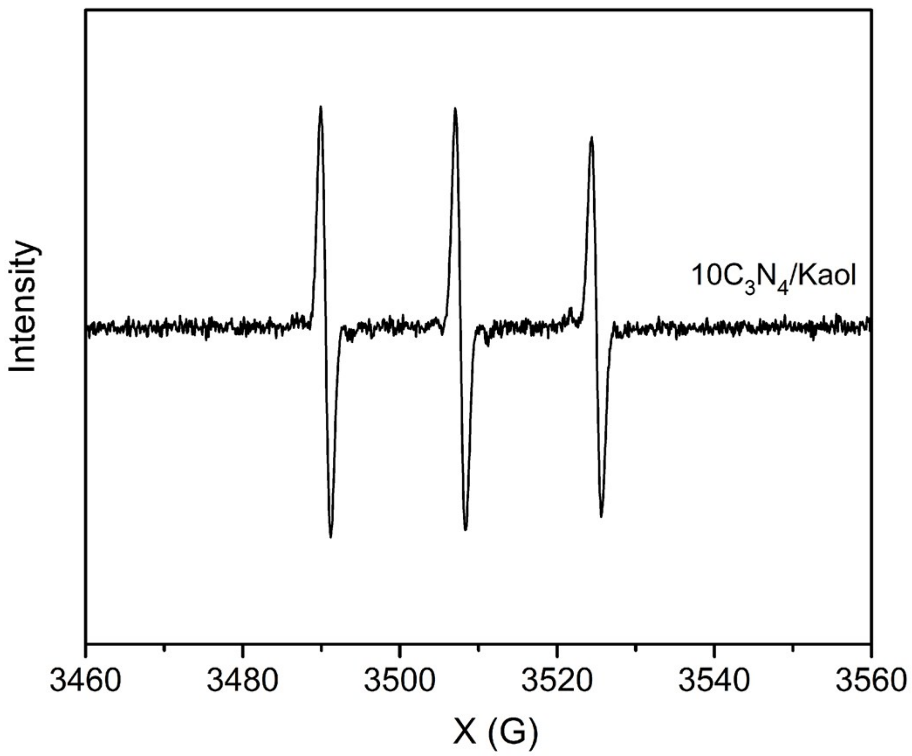

**Fig. S15** ESR spectrum of $10C_3N_4$/Kaol under visible light irradiation.

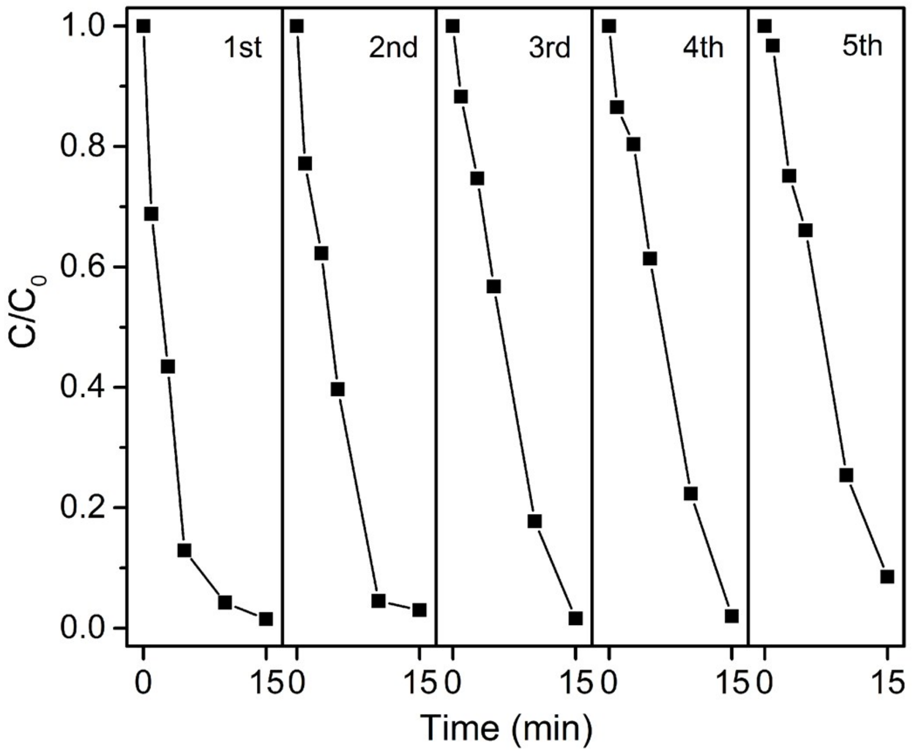

**Fig. S16** Recycle test of catalyst on Orang II degradation under visible light irradiation. Reaction conditions: [Orange II] = 50 mg/L, [PMS] = 0.5 g/L, [Catalyst (10$C_3N_4$/Kaol)] = 0.5 g/L.

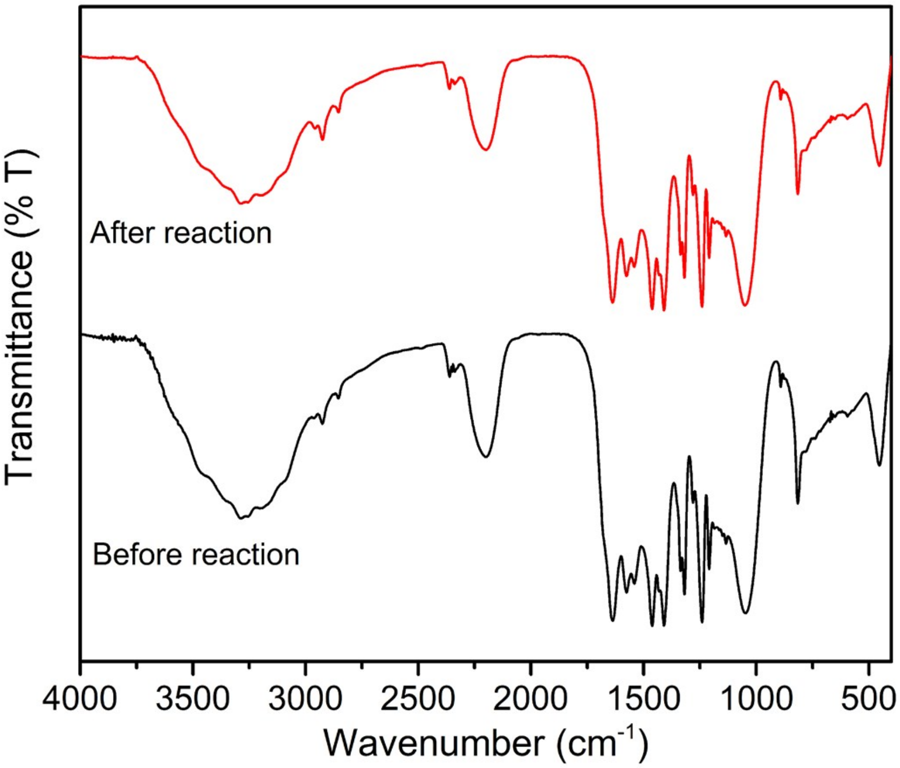

**Fig. S17** FTIR spectra of 10$C_3N_4$/Kaol photocatalysts before and after photocatalytic reaction.

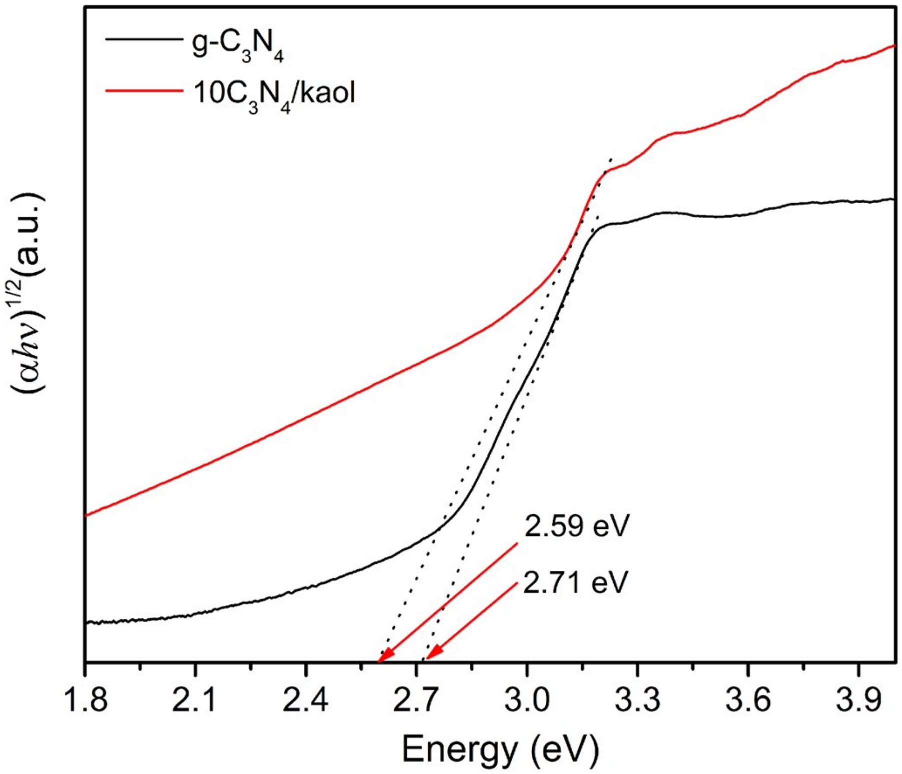

**Fig. S18** Kubelka–Munk plots of g-$C_3N_4$ and $10C_3N_4$/Kaol.

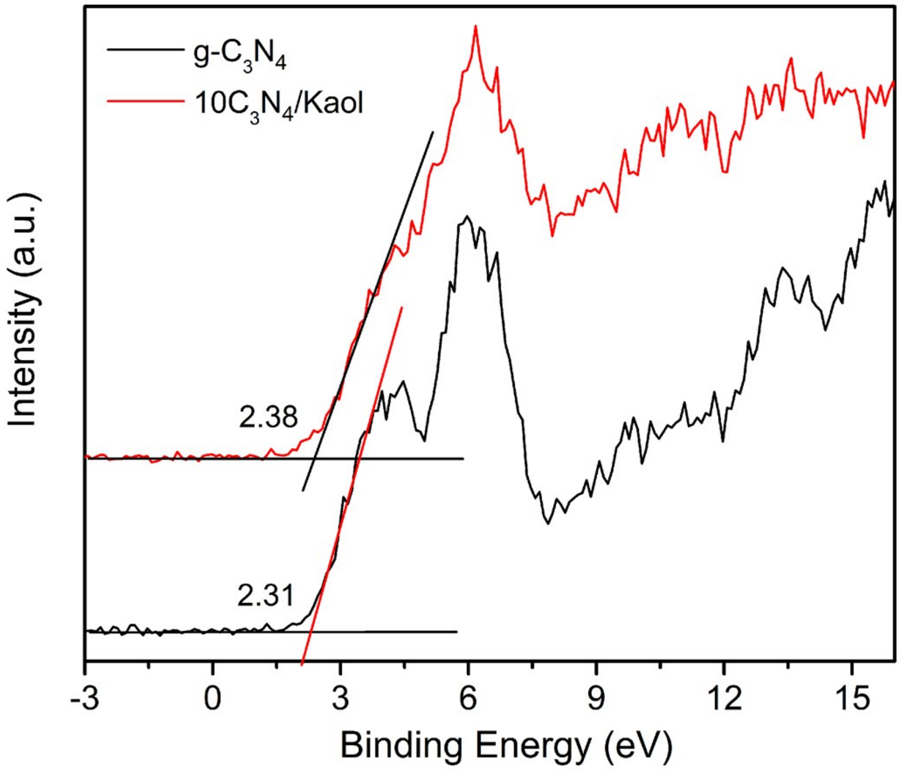

**Fig. S19** VB-XPS spectra of g-$C_3N_4$ and $10C_3N_4$/Kaol.

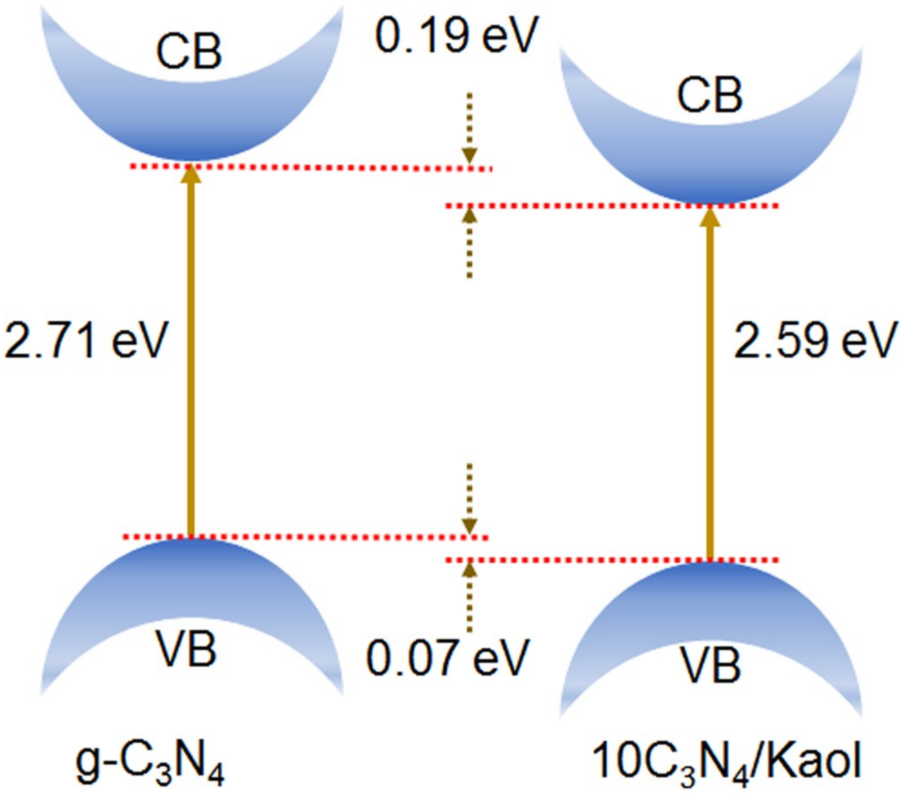

**Fig. S20** The schematic band structures diagrams of g-$C_3N_4$ and $10C_3N_4$/Kaol.

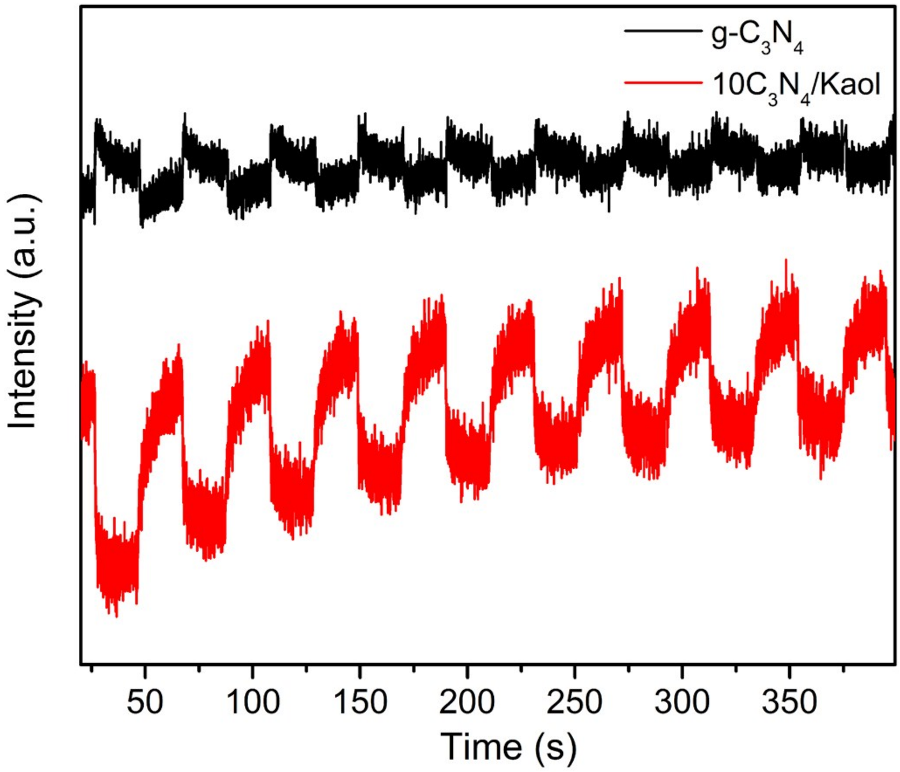

**Fig. S21** Transient photocurrent responses of g-$C_3N_4$ and $10C_3N_4$/Kaol with light on/off cycles.